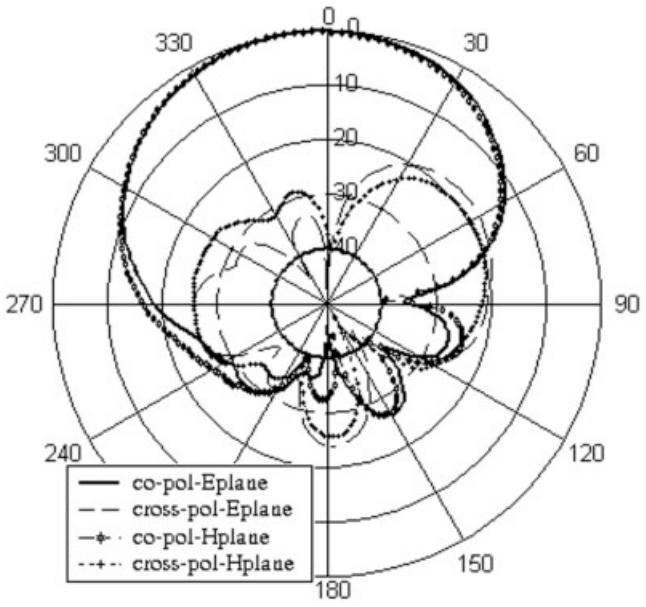

Figure 6 Measured radiation patterns of the three-turn concave hemispherical helical antenna at $C/\lambda = 1.04$

angular coverage and constant impedance are obtained. This antenna provides a 3-dB axial-ratio bandwidth of 13.5% and a peak gain of 9 dB. The obtained results make the proposed antenna suitable for satellite communications.

ACKNOWLEDGMENT

This work is supported by the Research Grant Council of Hong Kong SAR under grant no. 9040934.

REFERENCES

1. J.D. Kraus, Antennas for all applications, McGraw-Hill, New York, 2002.
2. A. Safaai-Jazi and J.C. Cardoso, Radiation characteristics of a spherical helical antenna, IEE Proc Microwave Antennas Propagat 143 (1996).
3. F. Weeratumanoon and A. Safaai-Jazi, Truncated spherical helical antennas, Electron Lett 36 (2000), 607–609.
4. H.T. Hui, K.Y. Chan, and E.K.N. Yung, The low-profile hemispherical helical antenna with circular polarization radiation over a wide angular range, IEEE Trans Antennas Propagat 51 (2003), 1415–1418.
5. R.F. Harrington, Field computation by moment method, IEEE Press, Piscataway, 1993.
6. H. Nakano, S. Okuzawa, K. Ohishi, H. Mimaki, and J. Yamauchi, A curl antenna, IEEE Trans Antennas Propagat 41 (1993), 1570–1575.
7. H. Nakano, Helical and spiral antennas: A numerical approach, Research Studies Press, Letchworth; Wiley, New York, 1987.
8. K.Y. Chan, H.T. Hui, and E.K.N. Yung, Central-fed hemispherical helical antenna, IEEE AP-S 4 (2001), 545–548.

UNIAXIAL DIELECTRIC MEDIA WITH HYPERBOLIC DISPERSION RELATIONS

Tom G. Mackay,[1] Akhlesh Lakhtakia,[2] and Ricardo A. Depine[3]

[1] School of Mathematics
University of Edinburgh
Edinburgh EH9 3JZ, United Kingdom

[2] CATMAS—Computational & Theoretical Materials Sciences Group
Department of Engineering Science and Mechanics
Pennsylvania State University
University Park, PA 16802-6812

[3] Grupo de Electromagnetismo Aplicado
Departamento de Fisica, Facultad de Ciencias Exactas y Naturales
Universidad de Buenos Aires
Ciudad Universitaria, Pabellón I
1428 Buenos Aires, Argentina

Received 10 August 2005

ABSTRACT: *Planewave propagation with hyperbolic/hyperboliclike characteristics in uniaxial dielectric media is investigated. The phase velocity is positive with respect to the time-averaged Poynting vector for both evanescent and nonevanescent propagation in nondissipative media. A conceptualization of a uniaxial medium, which exhibits hyperboliclike planewave characteristics as a homogenized composite medium, is presented.* © 2005 Wiley Periodicals, Inc. Microwave Opt Technol Lett 48: 363–367, 2006; Published online in Wiley InterScience (www.interscience.wiley.com). DOI 10.1002/mop.21350

Key words: *hyperbolic dispersion relations; elliptical dispersion relations; Bruggeman homogenization formalism*

1. INTRODUCTION

As the materials sciences and technologies continue their rapid development, realistic possibilities are emerging of realizing so-called metamaterials with novel and hitherto unconsidered optical/electromagnetic properties. A prime example is provided by the recently discovered metamaterials which support planewave propagation with negative phase velocity (NPV), and thereby negative refraction. Until 2000, little attention had been paid to the phenomenon of negative refraction. Since 2000, there has been an explosion of interest in negative refraction [1, 2], following experimental reports of a metamaterial which supports negative refraction in the microwave regime [3].

Naturally occurring uniaxial crystals have been extensively studied ever since the earliest days of the optical sciences. However, the electromagnetic properties of uniaxial media have recently been revisited by theoreticians in consideration of the prospects for NPV propagation in such media [4–7]. A closely related issue concerns uniaxial dielectric-magnetic media with indefinite constitutive dyadics [8, 9].

The defining characteristic of a uniaxial dielectric medium is a distinguished axis of symmetry, known as the optic axis. Mathematically, the permittivity dyadic of a uniaxial dielectric medium may be expressed as

$$\underline{\underline{\varepsilon}} = \varepsilon \underline{\underline{I}} + (\varepsilon_x - \varepsilon)\,\underline{\hat{x}}\,\underline{\hat{x}}, \tag{1}$$

where a coordinate system has been selected in which the direction of the optic axis coincides with the direction of the unit vector $\underline{\hat{x}}$ lying along the x axis, and $\underline{\underline{I}}$ denotes the 3×3 identity dyadic. The real-valued parameter

$$\gamma = \begin{cases} \dfrac{\varepsilon_x}{\varepsilon} & \text{for } \varepsilon_x,\ \varepsilon \in \mathbb{R} \\ \dfrac{\mathrm{Re}\{\varepsilon_x\}}{\mathrm{Re}\{\varepsilon\}} & \text{for } \varepsilon_x,\ \varepsilon \in \mathbb{C} \end{cases} \tag{2}$$

may be usefully employed to characterize planewave propagation in the medium specified by (1). The upper expression is appropriate for nondissipative media whereas the lower expression is appropriate for dissipative media.

The electromagnetic/optical properties of uniaxial media with $\gamma > 0$—this category includes most naturally occurring uniaxial crystals—have long been established. Comprehensive descriptions can be found in standard works [10, 11]. Uniaxial media with $\gamma < 0$ are much more exotic. Interest in these media stems from their potential applications in negatively refracting scenarios [8, 9] and in diffraction gratings [12], for example.

Planewave propagation in a uniaxial medium is characterized in terms of a dispersion relation which is quadratic in terms of the corresponding wavevector components. The dispersion relations for nondissipative media with $\gamma > 0$ have an elliptical representation, whereas a hyperbolic representation is associated with $\gamma < 0$. In this paper, we investigate the planewave characteristics and conceptualization of uniaxial dielectric media with hyperbolic dispersion relations.

2. PLANEWAVE ANALYSIS

The propagation of plane waves with field phasors

$$\left.\begin{aligned} \underline{E}(\underline{r}) &= \underline{E}_0 \exp(i\underline{k}\cdot\underline{r}) \\ \underline{H}(\underline{r}) &= \underline{H}_0 \exp(i\underline{k}\cdot\underline{r}) \end{aligned}\right\} \tag{3}$$

in the uniaxial dielectric medium specified by the permittivity dyadic (1) is investigated. The permittivity parameters are generally complex-valued, that is, $\varepsilon,\ \varepsilon_x \in \mathbb{C}$. The wavevector $\underline{k}$ is taken to be of the form

$$\underline{k} = \alpha\hat{\underline{x}} + \beta\hat{\underline{z}}, \tag{4}$$

where $\alpha \in \mathbb{R}$, $\beta \in \mathbb{C}$, and $\hat{\underline{z}}$ is the unit vector directed along the z-axis. This form of $\underline{k}$ is appropriate to planar boundary value problems [11] and from the practical viewpoint of potential optical devices [12]. We note that the plane waves (3) are generally nonuniform.

The source-free Maxwell curl postulates

$$\left.\begin{aligned} \nabla \times \underline{E}(\underline{r}) &= i\omega \underline{B}(\underline{r}) \\ \nabla \times \underline{H}(\underline{r}) &= -i\omega \underline{D}(\underline{r}) \end{aligned}\right\} \tag{5}$$

to yield the vector Helmholtz equation:

$$[(\nabla \times \underline{I}) \cdot (\nabla \times \underline{I}) - \mu_0 \omega^2 \underline{\underline{\varepsilon}}] \cdot \underline{E}(\underline{r}) = \underline{0}, \tag{6}$$

μ_0 is the permeability of free space. Combining (3) with (6) yields the planewave dispersion relation:

$$(\alpha^2 + \beta^2 - \varepsilon\mu_0\omega^2)(\alpha^2\varepsilon_x + \beta^2\varepsilon - \varepsilon_x\varepsilon\mu_0\omega^2) = 0. \tag{7}$$

In the following, we consider the time-averaged Poynting vector

$$\underline{P}(\underline{r}) = \frac{\exp(-2\,\mathrm{Im}\{\beta\}z)}{2\mu_0\omega}\,\mathrm{Re}\{|\underline{E}_0|^2\underline{k}^* - (\underline{E}_0\cdot\underline{k}^*)\underline{E}_0^*\}. \tag{8}$$

Evanescent plane waves are characterized by $\mathrm{Im}\{\beta\} > 0$. The scenario characterized by $\mathrm{Im}\{\beta\} < 0$ is not physically plausible for passive media, even of the negatively refracting kind [12, 13], and is therefore not considered here.

2.1. Ordinary Wave

The ordinary wavevector

$$\underline{k}_{or} = \alpha\hat{\underline{x}} + \beta_{or}\hat{\underline{z}} \tag{9}$$

arises from the dispersion relation (7) with components satisfying

$$\alpha^2 + \beta_{or}^2 = \omega^2\varepsilon\mu_0. \tag{10}$$

The vector Helmholtz Eq. (6) yields the eigenvector solution $\underline{E}_0 = E_y\hat{\underline{y}}$, and is directed parallel to the unit vector $\hat{\underline{y}}$ lying along the y-axis, where the complex-valued magnitude E_y is determined by the initial/boundary conditions. Consequently, the time-averaged Poynting vector reduces to

$$\underline{P}(\underline{r}) = \frac{\exp(-2\,\mathrm{Im}\{\beta_{or}\}z)}{2\omega\mu_0}\,|E_y|^2\mathrm{Re}\{\underline{k}_{or}^*\}. \tag{11}$$

Since

$$\mathrm{Re}\{\underline{k}_{or}\}\cdot\underline{P}(\underline{r}) = \frac{\exp(-2\,\mathrm{Im}\{\beta_{or}\}z)}{2\omega\mu_0}\,|E_y|^2[\alpha^2 + (\mathrm{Re}\{\beta_{or}\})^2] \geq 0, \tag{12}$$

we say that ordinary plane waves have positive phase velocity (PPV) for all directions of propagation.

Let us focus attention on a nondissipative medium (that is, ε, $\varepsilon_x \in \mathbb{R}$). From (10) we see that $\mathrm{Im}\{\beta_{or}\} \neq 0$ for (i) $\varepsilon > 0$ when $\omega^2\varepsilon\mu_0 < \alpha^2$ and (ii) $\varepsilon < 0$. Thus, nonevanescent ordinary plane waves propagate in a nondissipative medium only when $\varepsilon > 0$ and $-\omega\sqrt{\varepsilon\mu_0} < \alpha < \omega\sqrt{\varepsilon\mu_0}$. In geometric terms, the wavevector components have a circular representation in (α, β_{or}) space.

2.2. Extraordinary Wave

The extraordinary wavevector

$$\underline{k}_{ex} = \alpha\hat{\underline{x}} + \beta_{ex}\hat{\underline{z}}, \tag{13}$$

arises from the dispersion relation (7), with components satisfying

$$\alpha^2\varepsilon_x + \beta_{ex}^2\varepsilon = \omega^2\varepsilon\varepsilon_x\mu_0. \tag{14}$$

In the case where $\beta_{ex} = 0$, the mathematical description of the extraordinary wave is isomorphic to that for the ordinary wave. Therefore, we exclude this possibility from our consideration in this section. The eigenvector

$$\underline{E}_0 = \left(\hat{\underline{x}} - \frac{\varepsilon_x\alpha}{\varepsilon\beta_{ex}}\hat{\underline{z}}\right)E_x \tag{15}$$

arises as a solution to the vector Helmholtz Eq. (6); the complex-valued magnitude E_x is determined by the initial/boundary conditions. The corresponding time-averaged Poynting vector is given by

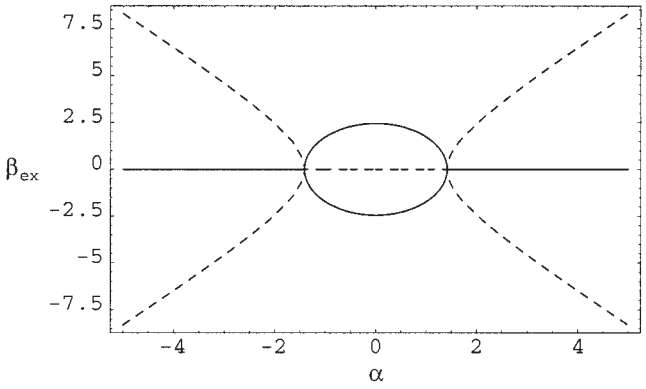

Figure 1 A plot of the real (solid curve) and imaginary (dashed curve) parts of β_{ex} against α for $\varepsilon_x = 6\varepsilon_0$ and $\varepsilon = 2\varepsilon_0$. The values of α and β_{ex} are normalized with repsect to $\omega\sqrt{\varepsilon_0\mu_0}$

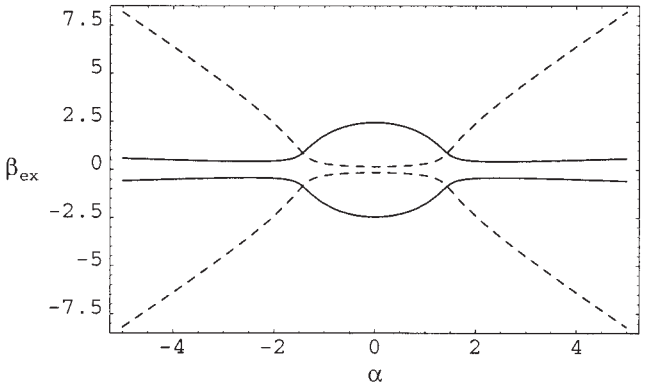

Figure 2 As in Fig. 1, but for $\varepsilon_x = (6 + i0.75)\varepsilon_0$ and $\varepsilon = (2 + i0.5)\varepsilon_0$

$$\underline{P}(\underline{r}) = \frac{\exp(-2\,\mathrm{Im}\{\beta_{ex}\}z)}{2\omega\mu_0}\mathrm{Re}\left\{\alpha\left(\left|\frac{\varepsilon_x}{\varepsilon\beta_{ex}}\right|^2\alpha^2 + \frac{\varepsilon_x\beta_{ex}^*}{\varepsilon\beta_{ex}}\right)\hat{\underline{x}} + \left(\beta_{ex}^* + \alpha^2\frac{\varepsilon_x^*}{\varepsilon^*\beta_{ex}^*}\right)\hat{z}\right\}|E_x|^2. \quad (16)$$

Hence, we obtain

$$\mathrm{Re}\{\underline{k}_{ex}\}\cdot\underline{P}(\underline{r}) = \frac{\exp(-2\,\mathrm{Im}\{\beta_{ex}\}z)}{2\omega\mu_0}\left[(\mathrm{Re}\{\beta_{ex}\})^2 + \alpha^2\left(\alpha^2\left|\frac{\varepsilon_x}{\varepsilon\beta_{ex}}\right|^2 + \mathrm{Re}\left\{\frac{\varepsilon_x\beta_{ex}^*}{\varepsilon\beta_{ex}}\right\} + \mathrm{Re}\{\beta_{ex}\}\mathrm{Re}\left\{\frac{\varepsilon_x^*}{\varepsilon^*\beta_{ex}^*}\right\}\right)\right]. \quad (17)$$

We analytically explore the nondissipative scenario for nonevanescent and evanescent planewave propagation in subsections 2.3. and 2.4., respectively, whereas both the dissipative and the nondissipative scenarios are treated graphically in subsection 2.5.

2.3. Nonevanescent Propagation

From Eq. (14), the inequality

$$\omega^2\varepsilon_x\mu_0 - \alpha^2\gamma > 0 \quad (18)$$

is satisfied for nonevanescent planewave propagation in a nondissipative medium, where γ is defined in (2). Thus, $\mathrm{Im}\{\beta_{ex}\} = 0$. We explore the cases $\gamma > 0$ and $\gamma < 0$ separately as follows.

(i) If $\gamma > 0$, then we require $-\omega\sqrt{\varepsilon\mu_0} < \alpha < \omega\sqrt{\varepsilon\mu_0}$ in order to comply with (18). This implies that $\varepsilon > 0$ and $\varepsilon_x > 0$. In geometric terms, the wavevector components have an elliptical representation in (α, β_{ex}) space.

(ii) If $\gamma < 0$, then the inequality (18) reduces to $\omega^2\varepsilon\mu_0 < \alpha^2$. Therefore, we see that nonevanescent propagation arises for (a) $\alpha > \omega\sqrt{\varepsilon\mu_0}$ and $\alpha < -\omega\sqrt{\varepsilon\mu_0}$ when $\varepsilon > 0$ and (b) $-\infty < \alpha < \infty$ when $\varepsilon < 0$. In geometric terms, the wavevector components have a hyperbolic representation in (α, β_{ex}) space.

For $\mathrm{Im}\{\beta_{ex}\} = 0$ and ε_x, $\varepsilon \in \mathbb{R}$, we find that (17) reduces to

$$\mathrm{Re}\{\underline{k}_{ex}\}\cdot\underline{P}(\underline{r}) = \frac{\omega^3\mu_0\gamma^2\varepsilon_x^2}{2\beta_{ex}^2}. \quad (19)$$

Hence, nonevanescent plane waves have PPV regardless of the sign of γ or ε_x.

2.4. Evanescent Propagation

We turn to evanescent planewave propagation in a nondissipative medium as characterized by the inequality

$$\omega^2\varepsilon_x\mu_0 - \alpha^2\gamma < 0. \quad (20)$$

Hence, we have $\mathrm{Re}\{\beta_{ex}\} = 0$. As in the previous subsection, we explore the cases $\gamma > 0$ and $\gamma < 0$ separately.

(i) If $\gamma > 0$, then the situation mirrors that which we described earlier for hyperbolic nonevanescent propagation. That is, evanescent propagation arises for (a) $\alpha > \omega\sqrt{\varepsilon\mu_0}$ and $\alpha < -\omega\sqrt{\varepsilon\mu_0}$ when $\varepsilon > 0$ and (b) $-\infty < \alpha < \infty$ when $\varepsilon < 0$. In geometric terms, the wavevector components have a hyperbolic representation in $(\alpha, \mathrm{Im}\{\beta_{ex}\})$ space.

(ii) If $\gamma < 0$, then evanescent propagation arises provided that $\varepsilon > 0$, $\varepsilon_x < 0$, and $-\omega\sqrt{\varepsilon\mu_0} < \alpha < \omega\sqrt{\varepsilon\mu_0}$. In geometric terms, the wavevector components have an elliptical representation in $(\alpha, \mathrm{Im}\{\beta_{ex}\})$ space.

For $\mathrm{Re}\{\beta_{ex}\} = 0$ and ε_x, $\varepsilon \in \mathbb{R}$, we find that (17) reduces to

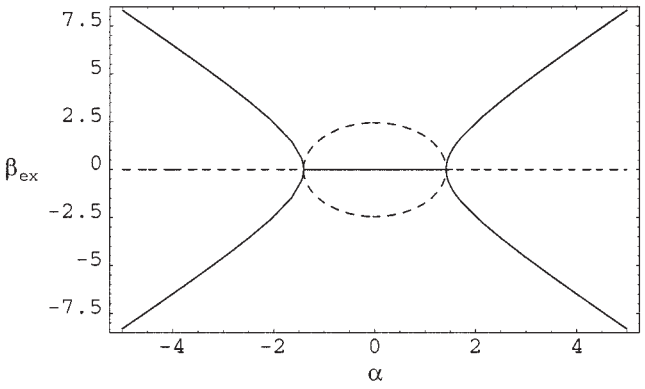

Figure 3 A plot of the real (solid curve) and imaginary (dashed curve) parts of β_{ex} against α for $\varepsilon_x = -6\varepsilon_0$ and $\varepsilon = 2\varepsilon_0$. The values of α and β_{ex} are normalized with respect to $\omega\sqrt{\varepsilon_0\mu_0}$

$$\mathrm{Re}\{\underline{k}_{ex}\}\cdot\underline{P}(\underline{r}) = \frac{\omega\alpha^2\varepsilon_x\gamma}{2(\alpha^2\gamma-\omega^2\mu_0\varepsilon_x)}\exp(-2\,\mathrm{Im}\{\beta_{ex}\}z). \quad (21)$$

Hence, evanescent plane waves have PPV if (a) $\gamma < 0$ or (b) $\gamma > 0$ and $\varepsilon_x > 0$. However, negative phase velocity (NPV) propagation arises if $\gamma > 0$ and $\varepsilon_x < 0$.

2.5. Illustrative Examples

Let us illustrate the geometric aspect of the dispersion relations with some representative numerical examples.

Firstly, suppose we consider the case $\gamma > 0$ with $\varepsilon = 2\varepsilon_0$ and $\varepsilon_x = 6\varepsilon_0$, where ε_0 is the free-space permittivity. In Figure 1 the real and imaginary parts of β_{ex} are plotted against α. The elliptical nonevanescent nature of the dispersion relation is clear for $-\omega\sqrt{2\varepsilon_0\mu_0} < \alpha < \omega\sqrt{2\varepsilon_0\mu_0}$, while the hyperbolic evanescent nature is apparent for $\alpha < -\omega\sqrt{2\varepsilon_0\mu_0}$ and $\alpha > \omega\sqrt{2\varepsilon_0\mu_0}$. The elliptical/hyperbolic geometric interpretation breaks down when dissipative media are considered. However, the corresponding dispersion relations are geometrically reminiscent of their nondissipative counterparts. This can be observed in Figure 2, in which the graphs corresponding to Figure 1 are displayed for $\varepsilon = (2 + i0.5)\varepsilon_0$ and $\varepsilon_x = (6 + i0.75)\varepsilon_0$.

Secondly, we turn to the case $\gamma < 0$ with $\varepsilon = 2\varepsilon_0$ and $\varepsilon_x = -6\varepsilon_0$. The real and imaginary parts of β_{ex} are graphed against α in Figure 3. The graphs mirror those of Figure 1 but with nonevanescent and evanescent aspects interchanged; that is, we observe hyperbolic nonevanescent characteristics for $\alpha < -\omega\sqrt{2\varepsilon_0\mu_0}$ and $\alpha > \omega\sqrt{2\varepsilon_0\mu_0}$, and elliptical evanescent characteristics for $-\omega\sqrt{2\varepsilon_0\mu_0} < \alpha < \omega\sqrt{2\varepsilon_0\mu_0}$. The corresponding graphs for $\varepsilon = (2 + i0.5)\varepsilon_0$ and $\varepsilon_x = (-6 + i0.75)\varepsilon_0$ are presented in Figure 4. Note that the shapes of the graphs in Figures 4 and 2 are similar but not identical.

3. CONCEPTUALIZATION VIA HOMOGENIZATION

Although uniaxial dielectric media with $\gamma < 0$ are not readily observed in nature,[§] they can be conceptualized as metamaterials by means of homogenization.

For example, let us consider the homogenization of a composite comprising two component materials phases, labelled as a and b. Both component material phases are taken to be isotropic dielectric media: ε^a and ε^b denote the permittivity scalars of phases a and b, respectively. The component material phases are envisioned as random distributions of identically-oriented, spheroidal particles. The spheroidal shape—which is taken to be the same for all spheroids in component material phase a and b—is parameterized via the shape dyadic $\underline{\underline{U}} = \mathrm{diag}(U_x, U, U)$. That is, we take the spheroid's principal axis to lie along the x axis. The spheroid's surface is prescribed by the vector

$$\underline{r}_s(\theta, \phi) = \eta\underline{\underline{U}}\cdot\hat{\underline{r}}(\theta, \phi), \quad (22)$$

with $\hat{\underline{r}}$ being the radial unit vector specified by the spherical polar coordinates θ and ϕ. The linear dimensions of the spheroid, as determined by the parameter η, are assumed to be small relative to the electromagnetic wavelength(s).

The permittivity dyadic of the resulting homogenized composite medium (HCM):

$$\underline{\underline{\varepsilon}}^{HCM} = \mathrm{diag}(\varepsilon_x^{HCM}, \varepsilon^{HCM}, \varepsilon^{HCM}), \quad (23)$$

[§] Note that bismuth, for example, exhibits $\gamma < 0$ at liquid-helium temperatures [14].

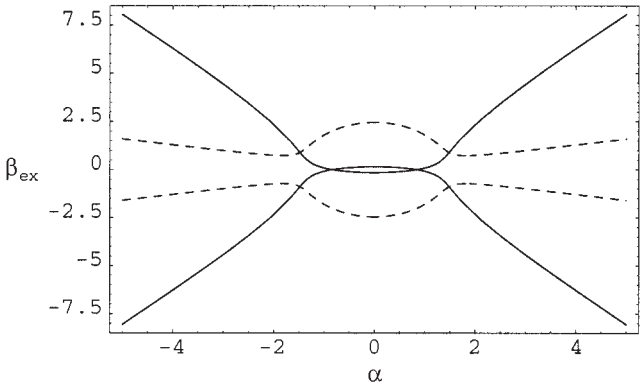

Figure 4 As in Fig. 3, but for $\varepsilon_x = (-6 + i0.75)\varepsilon_0$ and $\varepsilon = (2 + i0.5)\varepsilon_0$

as estimated using the Bruggeman homogenization formalism, is provided implicitly via

$$f_a\underline{\underline{a}}^a + f_b\underline{\underline{a}}^b = \underline{\underline{0}}, \quad (24)$$

where f_a and $f_b = 1 - f_a$ denote the respective volume fractions of the material component phases a and b. The polarizability dyadics in (24) are defined as

$$\underline{\underline{a}}^\ell = (\varepsilon^\ell\underline{\underline{I}} - \underline{\underline{\varepsilon}}^{HCM})\cdot[\underline{\underline{I}} + i\omega\underline{\underline{D}}\cdot(\varepsilon^\ell\underline{\underline{I}} - \underline{\underline{\varepsilon}}^{HCM})]^{-1}, \quad (\ell = a, b), \quad (25)$$

wherein the depolarization dyadic is given by the surface integral

$$\underline{\underline{D}} = \frac{1}{i\omega 4\pi}\int_0^{2\pi} d\phi \int_0^{\pi} d\theta \sin\theta \left(\frac{1}{\hat{\underline{r}}\cdot\underline{\underline{U}}^{-1}\cdot\underline{\underline{\varepsilon}}^{HCM}\cdot\underline{\underline{U}}^{-1}\cdot\hat{\underline{r}}}\right)\underline{\underline{U}}^{-1}\cdot\hat{\underline{r}}\hat{\underline{r}}\cdot\underline{\underline{U}}^{-1}. \quad (26)$$

Closed-form expressions for the depolarization dyadic for uniaxial media are available in terms of hyperbolic functions [17]. However, we note that these exact results are not valid for nondissipative media with $\gamma < 0$, and numerical evaluation of $\underline{\underline{D}}$ has to be resorted to.

The Jacobi iteration scheme

$$\underline{\underline{\varepsilon}}^{HCM}[P] = \mathcal{T}\{\underline{\underline{\varepsilon}}^{HCM}[p-1]\}, \quad (p = 1, 2, 3, \ldots), \quad (27)$$

where the operator $\mathcal{T}$ is defined via

$$\mathcal{T}\{\underline{\underline{\varepsilon}}^{HCM}\} = \{f_a\varepsilon^a[\underline{\underline{I}} + i\omega\underline{\underline{D}}\cdot(\varepsilon^a\underline{\underline{I}} - \underline{\underline{\varepsilon}}^{HCM})]^{-1} + f_b\varepsilon^b[\underline{\underline{I}} + i\omega\underline{\underline{D}} \cdot(\varepsilon^b\underline{\underline{I}} - \underline{\underline{\varepsilon}}^{HCM})]^{-1}\}\cdot\{f_a[\underline{\underline{I}} + i\omega\underline{\underline{D}}\cdot(\varepsilon^a\underline{\underline{I}} - \underline{\underline{\varepsilon}}^{HCM})]^{-1} + f_b[\underline{\underline{I}} + i\omega\underline{\underline{D}}\cdot(\varepsilon^b\underline{\underline{I}} - \underline{\underline{\varepsilon}}^{HCM})]^{-1}\}^{-1}, \quad (28)$$

may be employed to solve (24) for $\underline{\underline{\varepsilon}}^{HCM}$. Suitable initial values for the iterative scheme are provided by

$$\underline{\underline{\varepsilon}}^{HCM}[0] = (f_a\varepsilon^a + f_b\varepsilon^b)\underline{\underline{I}}. \quad (29)$$

For further details on the Bruggeman homogenization formalism, the reader is referred to [15, 16] and to references therein.

Let us consider the homogenization scenario wherein material component phase a is taken to be iron at the 670-nm free-space wavelength. Correspondingly, we take $\varepsilon^a = (-4.34 + i20.5)\varepsilon_0$. The material component phase b is assumed to be free space; that

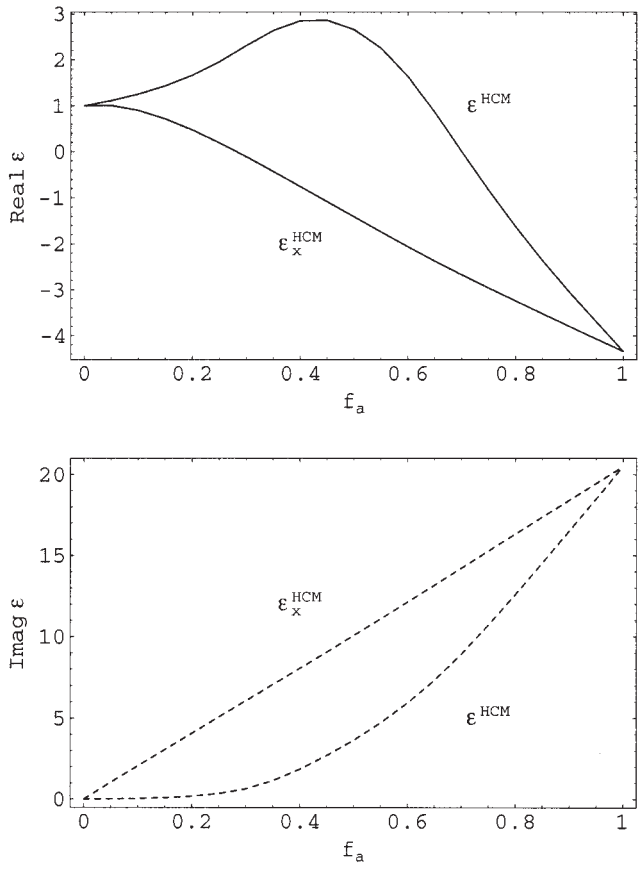

Figure 5 The real (above) and imaginary (below) parts of ε^{HCM} and ε_x^{HCM} plotted vs. volume fraction f_a. The permittivity values are normalized with respect to ε_0. Component phase values: $\varepsilon^a(-4.34 + i20.5)\varepsilon_0$ and $\varepsilon^b = \varepsilon_0$; spheroidal shape parameters: $U_x/U = 12$

is, $\varepsilon^b = \varepsilon_0$. The shape of the component spheroids is specified by $U_x/U = 12$. The Bruggeman estimates of the HCM permittivity parameters ε^{HCM} and ε_x^{HCM} are plotted as functions of volume fraction f_a in Figure 5. At intermediate values of f_a we see that $\gamma < 0$ for a substantial range of f_a values.

Extensive accounts of similar numerical homogenizations, based on the Bruggeman formalism and more general approaches, can be found elsewhere [15, 18].

4. CONCLUDING REMARKS

The dispersion relations for uniaxial dielectric media have been characterized with respect to the parameter γ of Eq. (2). For $\gamma < 0$, the dispersion relations are hyperbolic for nondissipative media and hyperboliclike for dissipative media. Similarly, the dispersion relations are elliptical for nondissipative media and elliptical-like for dissipative media with $\gamma > 0$. Through the homogenization of isotropic component material phases based on spheroidal topology, we have demonstrated that metamaterials with $\gamma < 0$ may be straightforwardly conceptualized. Thus, a practical means of achieving the exotic electromagnetic properties associated with hyperbolic and hyperboliclike uniaxial media has been presented.

REFERENCES

1. J.B. Pendry, Negative refraction, Contemp Phys 45 (2004), 191–202.
2. S.A. Ramakrishna, Physics of negative refractive index materials, Rep Progr Phys 68 (2005), 449–521.
3. R.A. Shelby, D.R. Smith, and S. Schultz, Experimental verification of a negative index of refraction, Sci 292 (2001), 77–79.
4. M.K. Kärkkäinen, Numerical study of wave propagation in uniaxially anisotropic Lorentzian backward-wave slabs, Phys Rev E 68 (2003), 026602.
5. Z. Liu, J. Xu, and Z. Lin, Omnidirectional reflection from a slab of uniaxially anisotropic negative refractive index materials, Opt Commun 240 (2004), 19–27.
6. L. Yonghua, W. Pei, Y. Peijun, X. Jianping, and M. Hai, Negative refraction at the interface of uniaxial anisotropic media, Opt Commun 246 (2005), 429–435.
7. L.I. Perez, M.T. Garea, and R.M. Echarri, Isotropic-uniaxial crystal interfaces: negative refraction and backward wave phenomena, Opt Commun (to appear).
8. D.R. Smith and D. Schurig, Electromagnetic wave propagation in media with indefinite permittivity and permeability tensors, Phys Rev Lett 90 (2003), 077405.
9. D.R. Smith, P. Kolinko, and D. Schurig, Negative refraction in indefinite media, J Opt Soc Am B 21 (2004), 1032–1043.
10. M. Born and E. Wolf, Principles of optics, 6th ed., Pergamon Press, Oxford.
11. H.C. Chen, Theory of electromagnetic waves, McGraw-Hill, New York, 1983.
12. R.A. Depine and A. Lakhtakia, Diffraction by a grating made of a uniaxial dielectric-magnetic medium exhibiting negative refraction, New J Physics 7 (2005), 158.
13. R.A. Depine and A. Lakhtakia, Perturbative approach for diffraction due to a periodically corrugated boundary between vacuum and a negative phase-velocity material, Opt Commun 233 (2004), 277–282.
14. V.A. Podolskiy, L. Alekseev, and E.E. Narimanov, Strongly anisotropic media: the THz perspectives of left-handed materials, http://www.arxiv.org/physics/0505024.
15. J.A. Sherwin, A. Lakhtakia, and B. Michel, Homogenization of similarly oriented, metallic, ellipsoidal inclusions using the Bruggeman formalism, Opt Commun 178 (2000), 267–273.
16. T.G. Mackay, Homogenization of linear and nonlinear complex composite materials, W.S. Weiglhofer and A. Lakhtakia (Eds.), Introduction to complex mediums for optics and electromagnetics, SPIE Press, Bellingham, WA, 2003, pp. 317–345.
17. B. Michel, A Fourier space approach to the pointwise singularity of an anisotropic dielectric medium, Int J Appl Electromag Mech 8 (1997), 219–227.
18. T.G. Mackay, A. Lakhtakia, and W.S. Weiglhofer, Homogenisation of similarly oriented, metallic, ellipsoidal inclusions using the bilocally approximated strong-property-fluctuation theory, Opt Commun 197 (2001), 89–95.

ACTIVE INTEGRATED ANTENNA USING T-SHAPED MICROSTIP-LINE-FED SLOT ANTENNA

Dong-Hyuk Choi and Seong-Ook Park
School of Engineering
Information and Communications University (ICU)
Daejeon, Korea

Received 6 August 2005

ABSTRACT: *An active integrated antenna (AIA), which consists of a T-shaped microstrip-line-fed slot antenna, is proposed. Since the designed antenna has an electromagnetically coupled feedback loop, it can easily solve the problem of DC isolation between ports of the amplifier. The fabricated parallel feedback antenna oscillator shows stable oscillation at a frequency of 10.05 GHz. The measured EIRP is 37.79 mW, and the cross-polarization levels are at least −15-dB lower than those of co-polarization for all directions.* © 2005 Wiley Periodicals, Inc. Microwave Opt Technol Lett 48: 367–370, 2006; Published online in Wiley InterScience (www.interscience.wiley.com). DOI 10.1002/mop.21351